Chemical Science

ROYAL SOCIETY OF CHEMISTRY

REVIEW

View Article Online
View Journal | View Issue

Cite this: *Chem. Sci.*, 2022, **13**, 8924

Fabrication of graphene-based porous materials: traditional and emerging approaches

Heidi Jahandideh, [ab] Jun-Ray Macairan,[a] Aram Bahmani,[c] Mathieu Lapointe[a] and Nathalie Tufenkji *[ab]

The anisotropic nature of 'graphenic' nanosheets enables them to form stable three-dimensional porous materials. The use of these porous structures has been explored in several applications including electronics and batteries, environmental remediation, energy storage, sensors, catalysis, tissue engineering, and many more. As method of fabrication greatly influences the final pore architecture, and chemical and mechanical characteristics and performance of these porous materials, it is essential to identify and address the correlation between property and function. In this review, we report detailed analyses of the different methods of fabricating porous graphene-based structures – with a focus on graphene oxide as the base material – and relate these with the resultant morphologies, mechanical responses, and common applications of use. We discuss the feasibility of the synthesis approaches and relate the GO concentrations used in each methodology against their corresponding pore sizes to identify the areas not explored to date.

Received 28th March 2022
Accepted 4th July 2022

DOI: 10.1039/d2sc01786e

rsc.li/chemical-science

1. Introduction

Space is one of the dimensions that is often sought after not only by humans but also by nature. If we increase the surface area without compromising the other properties of interest, we can claim to have improved the structure. Sea corals are an interesting example found in nature with enhanced space and surface area owing to their porous structures. After millions of years that nature has spent optimizing its structures, this challenge has become the ultimate goal in many research areas. Owing to their outstanding surface to volume ratios,[1] porous materials are of great interest in many different applications where they facilitate interactions with other atoms, ions, and molecules. Porous solids have drawn interest from chemists, engineers, materials scientists, and other researchers as they can serve as catalysts,[2] adsorbents,[3] membranes,[4] and filters,[5] to name a few. Fabrication of free-standing three-dimensional (3D) porous media heavily relies on the intermolecular interactions of the components as well as their robustness in tolerating the processing conditions. Therefore, not all materials can be implemented in constructing such media, and careful selection of building materials is a key criterion. With its introduction to the world of materials design, graphene oxide (GO) has attracted enormous attention from researchers across the globe.[6–9] This two-dimensional (2D) carbon-based, ideally monoatomic nanosheet is decorated with oxygen-containing moieties providing it with appealing properties.[10] Modifying GO into reduced graphene oxide (rGO) can not only tune the surface chemistry of this nanomaterial, but also provide it with the conductivity and electrical properties that are ideal for several applications.[11–14] It is worth noting that the porosity of graphene-based materials may arise from the inherent defects within graphenic nanosheets,[13,15] nanosheets' wrinkles and their self-assembly into 3D micro- and macrostructures.[2,16,17] With its specific surface area and storage modulus being two of the highest values reported at ~2600 m^2 g^{-1} and 130 GPa, respectively, researchers have taken advantage of this nanomaterial by incorporating it in the facile fabrication of porous materials for different applications including electronics and batteries,[18,19] energy storage,[20,21] water treatment,[22,23] tissue engineering[24] and many more (Fig. 1a). As seen in Fig. 1a, there have been thousands of articles and books published on the use of graphene-based porous materials to date and this number increases continuously, making it challenging for researchers to stay updated on their area of interest. Therefore, several researchers and scientists have provided comprehensive reviews on the use of graphene-based porous materials with a focus on specific applications: electronics and batteries,[19,25] energy storage,[26–28] water treatment and desalination,[29–31] and bone tissue engineering.[32,33]

Herein, we critically review the approaches employed in the development of graphene-based 3D porous materials to support scientists and engineers in the development of new materials. Methodologies reviewed are: (i) solvothermal process, (ii)

[a]*Department of Chemical Engineering, McGill University, Montreal, QC H3A 0C5, Canada. E-mail: nathalie.tufenkji@mcgill.ca*

[b]*McGill Institute for Advanced Materials (MIAM), McGill University, Montreal, Quebec, Canada*

[c]*Department of Mechanical Engineering, McGill University, Montreal, QC H3A 0C3, Canada*

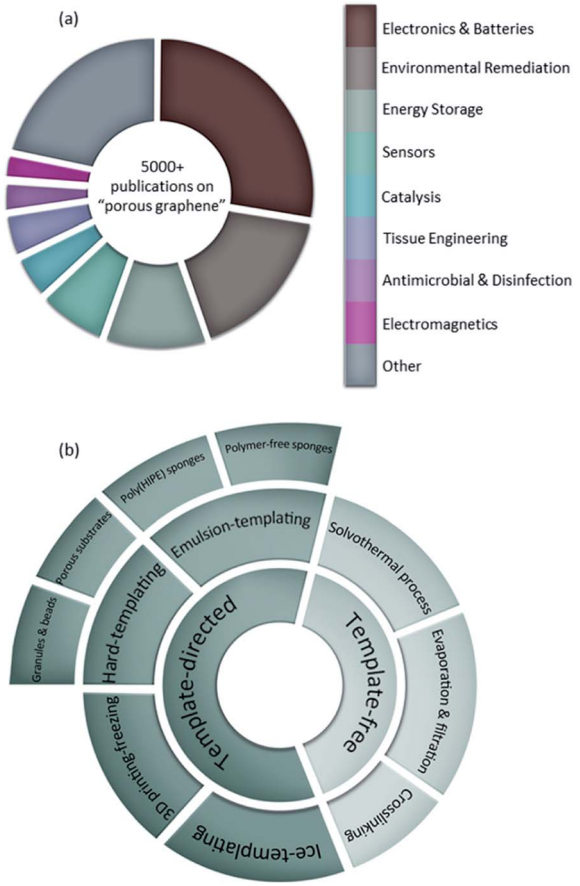

Fig. 1 (a) Publications on the use of porous graphene-based materials in various applications. Data obtained from Web of Science using the search query: "TI = ((porous OR aerogel OR hydrogel OR sponge* OR scaffold*) AND graphene). The size of each segment in the donut chart correlates to the number of publications with the assigned colour code. (b) Classification of methods studied in this review.

evaporation and filtration, (iii) cross-linking, (iv) ice-templating, (v) 3D printing-freezing, (vi) hard-templating, and (vii) emulsion-templating, which are classified into template-free and template-directed methods (Fig. 1b). The main goal of this review is to outline the different approaches to create graphene-based porous materials with a focus on those using graphene oxide as the base material, as well as highlighting the link between the methodologies used and the resulting properties that ultimately dictate the potential applications of use. A comprehensive feasibility analysis of the studied strategies is also provided for those interested in scaling up these graphene-based porous media.

Porosity scale bars are found to be categorized differently within the literature body causing some confusion and miscommunication among scientists. Considering the range of pore sizes found in porous graphene-based structures, the following classification of pore diameters (d) is used in this review to maintain a universal terminology: nanopores (0.1 nm < d < 0.1 μm), micropores (0.1 μm < d < 0.1 mm) and millipores (0.1 mm < d < 0.1 m). It is worth noting that this classification is different than the one used by the International Union of Pure and Applied Chemistry (IUPAC) but aligns with the common nomenclature used in most published articles in the field.

2. Template-free formation of graphene-based porous materials

In the formation of materials without templates, there is a strong reliance on the self-assembly of components, which is a consequence of their interactions.[34–37] With their unique structure and properties, graphene-based nanosheets have garnered significant attention as a versatile building block for this approach, thus resulting in novel 3D materials with interesting functionalities. The self-assembly of the nanosheets is driven by various weak interactions such as van der Waals, hydrogen bonding and π–π interactions.[38–40] These interactions lead to components forming the walls while repulsions, or steric hindrances and macroscopic wrinkles, lead to separation forming the "pores" of a porous material. Since there is no template in place in this method, we have minimal control over the pore sizes and shapes obtained. However, the concentration of the compounds used and processing conditions can influence the pore density and wall thickness of the resulting macrostructures.[41]

2.1. Solvothermal process

Solvothermal processes are among the most common bottom-up syntheses for nanomaterials. In solvothermal syntheses, desired precursors are dispersed in a solvent and sealed in a closed system at high temperature and pressure (*i.e.*, an autoclave), where the temperature is often higher or close to the boiling point of the solvent.[42] At the end of this process, the final products precipitate at the bottom of the autoclave. Common solvents include water, ethanol, thiourea, ammonia, ethylene glycol, hydrochloric acid, among others.[43] The process is termed hydrothermal if the solvent used is water.[38] This technique provides many advantages over other methods: (i) it is typically non-toxic depending on the solvent used, (ii) it is cost effective, (iii) it often yields very little unwanted by-products, and (iv) it requires a simple setup (generally a one-step procedure).

GO nanosheets are reduced by losing their oxygen-containing moieties at elevated temperatures (Fig. 2a). Solvothermal-mediated reduction of GO nanosheets leads to an increase in the π–π and hydrophobic interactions resulting in stacking of the sheets, thus self-assembling into a sponge. It is crucial that the concentration of GO be at a saturated level such that the GO nanosheets are at close distance resulting in sufficient cross-linking through overlaps of the nanosheets to generate a 3D network with pore sizes ranging from submicron to several microns (Fig. 2b).[21,38] Reaction time and temperature are key parameters for the solvothermal-mediated self-assembly of graphene-based sponges. With increase in reaction time, the resulting sponge decreases in size (as shown in Fig. 2c) with an increase in mechanical strength due to the prolonged opportunity for the nanosheets to form more crosslinking sites.[38] Generally, the temperature is greater than 150 °C in order to effectively reduce GO. In addition to promoting the removal of

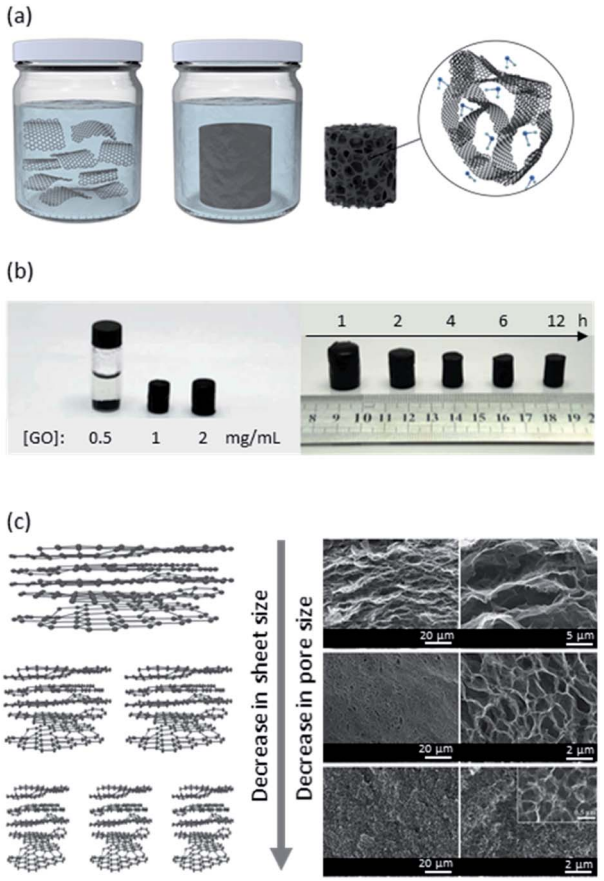

Fig. 2 (a) Schematic illustration of a typical solvothermal process. GO sheets are randomly oriented when dispersed in proper solvent but self-assemble upon their reduction into rGO and form a hierarchically porous material. The molecules surrounding the rGO nanosheets are water molecules. Schematic is not to scale. (b) Higher GO content yields a larger rGO sponge, as expected, and a longer reduction reaction time reduces the nanosheets further, leading to a smaller more stacked and less porous sponge. (c) The smaller the sheets' sizes, the smaller the pore sizes are in a porous graphene-based material. (b) is adapted with permission from ref. 38 © 2010 American Chemical Society. SEM images in (c) are adapted with permission from ref. 41 © 2016 Royal Society of Chemistry.

functional groups (such as C=O carboxyl and carbonyl groups),[44] high temperatures also increase the mobility of GO nanosheets, leading to a greater chance of interactions.[17] The high temperature is also responsible for an increase of pressure in the reaction vessel, which in turn facilitates the deoxygenation process and exfoliates the nanosheets with crumpled structural features. If desired, the resulting material can undergo freeze-drying to remove the captured water post-synthesis. This method results in the presence of a variety of pore sizes: micropores and nanopores. While the large pore sizes are a result of fabrication process and are process-dependent, the smaller pores are either dictated by the stacking, entanglement and overlap of GO nanosheets (2–50 nm pore sizes), or are a result of the defects in the nanosheets (<2 nm).[45] Without any additives, the size of the nanosheets is a critical parameter that governs the overall size of the pores (Fig. 2c). In general, the larger the GO nanosheets used in the reaction, the larger the resulting pore size in the graphene-based sponge, which is accompanied by a change in macrostructure morphology. Larger GOs induce an anisotropic flat slit-like pore structure, whereas smaller GOs generate nano-sized pores with an isotropic cage-like morphology.[41]

In solvothermal syntheses (much like in other methods to follow), the spacing between GO nanosheets is influenced by the degree of oxidation. The lower the oxygen content of the starting GO, the tighter the distance between the nanosheets.[44] More oxygenated functional groups allow for more water to be absorbed through hydrogen bonding during the film formation resulting in an increased interlayer distance to accommodate the presence of water molecules. The pH of the reaction mixture can dictate the overall chemical structure and the structural integrity of these sponges. There is a greater degree of reduction in basic pH where carbonyl groups are more easily removed through decarboxylation *via* nucleophilic attack of water.[46] This interaction yields the generation of CO_2 gas, a by-product of solvothermal treated GO. This gas can be entrapped in the sponges causing macroscopic voids. However, this can be mitigated through the addition of reagents, such as ammonia, which can convert the CO_2 into ionic species and can also create defects that allow the gas to escape the structure.[46] Thiourea can also be used in the formation of additional pores and strengthen the overall structural integrity of graphene-based sponges. During the hydrothermal process, thiourea can reduce GO nanosheets and form additional functional groups, namely amino ($-NH_2$) and sulfonic acid ($-SO_3H$).[47] These groups provide additional crosslinking between nanosheets resulting in the formation of compact porous sponges with good structural stability.

Graphene-based porous materials prepared *via* solvothermal-assisted reaction methods can be used in energy storage as supercapacitors. This is mainly due to their high surface area and low density, allowing for greater interaction with ions and electrons. The resulting materials possess ideal capacitive characteristics such as high gravimetric specific capacitance (up to 196 G g^{-1} for a 42 μm thick electrode), elevated areal specific capacitance (up to 402 mF cm^{-2} for 185 μm thick electrode) and low current leakage.[21,38,48] These sponges have also shown promise in environmental nanotechnology.[23,41] It is demonstrated that oils, such as dodecane, can be effectively absorbed into the sponge pores; thus, removing them from contaminated water. This is due to the inherently hydrophobic nature of rGO nanosheets and the overall macrostructure. Organic solvents can also be absorbed into the rGO sponges as they retain some of their moieties during the partial reduction of GO nanosheets.

2.2. Evaporation and filtration

Methods have been established that involve solvent evaporation or filtration of a GO dispersion to form membranes and films (Fig. 3a). The common approaches consist of vacuum filtration, layer-by-layer assembly, and drop-casting.[49–53] The resulting materials mainly comprise of (i) nanoporous single-layered

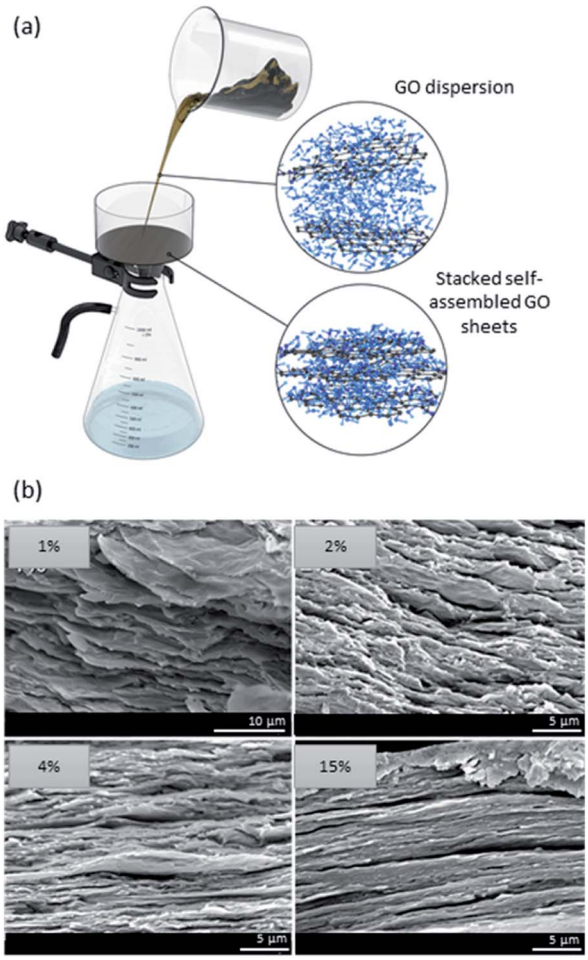

Fig. 3 (a) Schematic illustration of a filtration setup showing the randomness of and the distance between GO sheets. Once filtered, the nanosheets self-assemble into stacked porous 3D films. (b) SEM micrographs of a GO/alginate film prepared by means of evaporation. As displayed, higher GO content results in a more stacked and less porous 3D film. SEM images are adapted with permission from ref. 39 © 2019 American Chemical Society.

films, where the porosity is a consequence of defects, and (ii) stacked 3D films, where porosity is a result of both wrinkles and defects.[54–57] While there are attractive interactions between the nanosheets (*e.g.*, van der Waals), the challenge arises from edge-to-edge electrostatic repulsion that can hinder the overall stacking of the sheets.[57] There is a great interest for the use of graphene-based nanomaterials in separation technologies due to their inherent permeability and selectivity, which stem from nanochannels or "graphenic" defects.[58] The formation of 3D stacked graphene-based films through evaporation and layering is often done *via* self-assembly or vacuum filtration.[59,60] Moreover, in 3D films, the interlayer spacing is dictated by the alignment of nanosheets and their lamellar structures. Selectivity of such materials is size-dependent; small particulates and ions may pass through the channels while larger molecules are retained. For instance, once immersed in water, the hydration layer around GO nanosheets increases the interlayer spacing to ~0.45 nm allowing monovalent ions to pass while retaining larger divalent ions (*e.g.*, size > 0.45 nm).[61]

Many parameters are at play when designing GO-based films. Firstly, the thickness of the membrane is factored in the separation performance of GO films. Secondly, despite sub-angstrom differences in size, it is noted that the ion transport is dependent on the inter-layer spacing formed between the GO nanosheets in thicker membranes. On the other hand, the ion transport rate in thin membranes is solely dependent on pore sizes.[55] Thus, increasing the layers of GO nanosheets enhances molecular selectivity in detriment of permeability.[62,63] Therefore, when designing the material, precise control of the stacking of the sheets is vital in order to achieve a good balance of selectivity and permeability for optimal separation performance. The fabrication of GO-based membranes is also impacted by the GO content used. It has been demonstrated that the amount of gas channels increased as a function of increasing GO content up until a "critical point" where a drop in selectivity and gas permeability occurs, thus hindering its separation performance.[49] Generally, the higher the concentration of GO, the more tightly packed and well-ordered the nanosheets are; on the other hand, when GO concentrations are too low, there is a mixture of domains of disordered and highly aligned GO (Fig. 3b).[39] However, when GO content is too elevated, both the permeability and selectivity of the membrane are negatively impacted due to the formation of aggregates. In this instance, the molecular transport bypasses the nanochannels through membrane cracks and microscale defects.[64] The size of GO nanosheets also influences the formation of the material. Commonly, the larger the lateral size of GO nanosheets, the greater the permeability and selectivity of the membrane. This is governed by the formation of longer channels that allow for enhanced selectivity.[49] However, large GO nanosheets (*e.g.* >5 μm) suffer from poor dispersion and are susceptible to aggregation, which in turn hinders the separation capabilities of the film. Much research has been conducted on tuning the interlayer spacing in GO membranes *via* layer-by-layer assembly of different compounds in between GO nanosheets. These assemblies are driven either by covalent bonds, electrostatic interactions, or a combination of both.[65,66] The synergy of the intercalating compound or nanoparticle with the graphene matrix allows for improved membrane permeability because of the enlargement of nanochannels.

One of the challenges faced when fabricating a flat, membrane-like GO-based material is the lack of ductility originating from the intrinsic brittleness of GO.[67] The inherent flat structural simplicity can be limiting when more complex nonpolar structures are desired. More recently, researchers have been able to tackle this issue by simply mixing the GO with milled cellulose fibers.[67] It has been reported that even though the addition of fibers has reduced membranes' storage modulus, it has significantly improved their ductility. This newly explored technique is shown to be a low-cost method to effectively increase the deformability of vacuum-filtered GO membranes extending their applications to nonpolar structures.[67]

2.3. Crosslinking

Addition of different crosslinkers such as metal oxides, noble metals, divalent ions, monomers, or polymers to GO dispersions increases the viscosity of the final mixture, enabling self-assembly of the nanosheets into a 3D network.[68–71] Promotion of gelation can be achieved by both mixing (*i.e.*, physical crosslinking) and covalently grafting these components onto GO nanosheets (*i.e.*, chemical crosslinking).[72] Fig. 4 schematically compares the two physical and chemical crosslinking strategies. Briefly, the former mainly relies on intermolecular interactions (van der Waals interactions, hydrogen bonding, electrostatic forces, *etc.*) without forming a chemical bond, while the latter refers to the formation of a covalent bond between two components, and thus, is a stronger attachment but requires a more rigorous procedure. Moreover, as Fig. 4 shows, a polymer chain (polyacrylamide (PAM), in this case) can have multiple sites involved in different intermolecular interactions (*i.e.*, physical crosslinking). However, covalently bonding polymer chains onto GO nanosheets involves one site due to steric hindrance. Additionally, having multiple polymer chains chemically bonded reinforces the stiffness and mechanical strength of the final composite/hydrogel.

Au, Ag, Pd, Pt, Rh, and Ir are some of the metal particles proven to act as crosslinkers capable of enhancing storage modulus and yield stress values of the resultant 3D structures while yielding a low density (0.03 g cm^{-3}).[73] Examples of divalent ions that have been used as crosslinkers include Ca^{2+}, Ni^{2+} and Co^{2+}.[74] Formation of 3D macrostructures as a result of strong electrostatic interactions is another type of physical crosslinking. Since GO and rGO nanosheets are both negatively charged, they interact strongly with positively charged components (*e.g.*, chitosan and other molecules containing amino groups).[75–77] Additionally, hydrogen-bonding and electron–donor–acceptor interactions have been reported to result in formation of GO-based complexes leading to 3D macrostructures at concentrations where a percolated network is formed.[78] Covalently bonding different components, such as PAM and chitosan onto GO nanosheets, forms GO-based porous materials with improved mechanical responses (*e.g.*, storage modulus and yield stress values).[79–85] Porosity and pore architecture of crosslinked porous materials are functions of GO nanosheets' sizes, pH values of the used dispersions and the concentration of each component. Smaller GO nanosheets, lower pH and higher concentrations lead to the formation of smaller pores with thicker walls. Depending on the desired application, different molecules and ions can be selected as candidates to crosslink with GO/rGO nanosheets.[72] Metal oxides and noble metals cross-linkers enhance electrical properties of the final product while divalent ions and polymers are more effective in improving mechanical properties of these 3D macrostructures, making them more robust.[4,72,86,87]

3. Template-directed formation of graphene-based porous materials

Templating nanomaterials into porous materials prevents the formation of random void spaces and grants some control over the sizes and shapes of the pores as the thickness and sturdiness of the walls are somewhat predictable and tunable, depending on the components of the structure and the templates used. In this section, we describe the most common template-directed approaches used to form GO-based sponges.

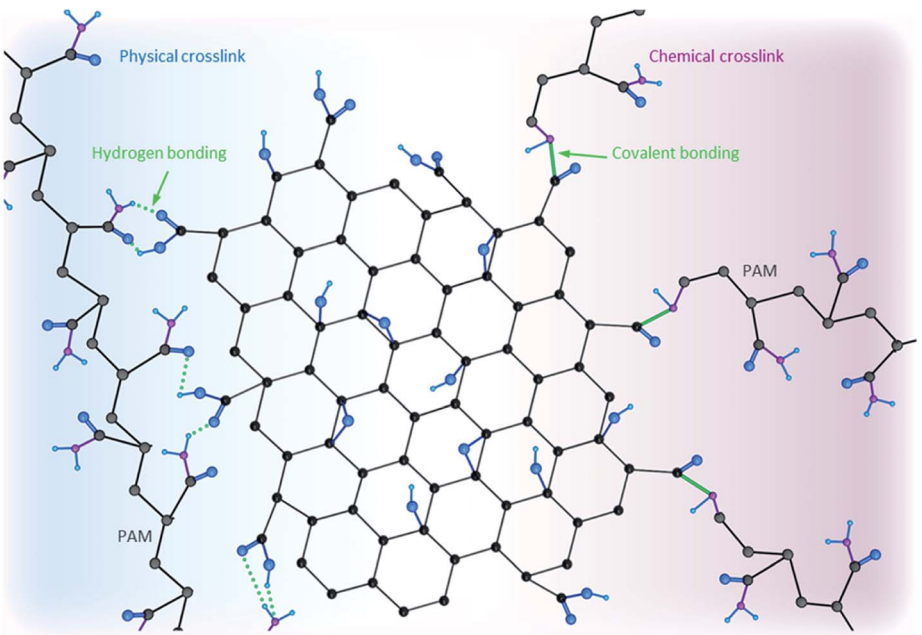

Fig. 4 Typical schematic representations of: (left) a physical cross-linking between a polyacrylamide (PAM) chain and a GO nanosheet originating solely from intermolecular interactions such as hydrogen bonding, and (right) a chemical cross-linking between a PAM molecule and a GO nanosheet which is a consequence of covalent bonding.

3.1. Ice-templating

A dispersion of GO, which may also include other components such as cellulose nanocrystals (CNCs) and other polymers as reinforcers, can be frozen by reducing the temperature. During this process, as ice crystals form, they pave the way for the assembly of solid particles within the system.[88] Bulk, unidirectional and bidirectional freeze-drying are the three types of lyophilization techniques where the dispersion of interest gets frozen using liquid nitrogen or argon.[89]

As shown in Fig. 5a, in the bulk freeze-drying, the container is fully immersed in liquid nitrogen and ice crystals are formed and grow randomly throughout the sample, starting near the walls of the container. This is the most common approach out of the three lyophilises employed in forming porous materials. Freeze-drying mixtures of GO with different polymers, such as PAM,[81] chitosan,[89,90] *etc.* has been used to form hydrogels and aerogels for a range of applications with pores ranging from several to tens of micrometers in size. The randomness of pores can be seen in both top- and cross-sectional side-views of the SEM images shown in Fig. 5b. By adjusting the rate of ice crystal formation and its direction, we can control the morphology of this type of porous scaffold. To do so, the vial or jar containing the dispersion of interest is placed in an insulating container (*e.g.*, Styrofoam), over liquid nitrogen, allowing for the ice crystals to form and grow from the bottom to the top creating continuous microchannels as a result of ordered pores (Fig. 5c).[91] While top-view SEM images reveal the presence of similar pore sizes to those found in bulk freeze-dried sponges, we can observe the creation of ordered porosity and microchannels in a cross-sectional side-view micrograph (Fig. 5d). As the third strategy to freeze-dry graphene-based materials, bidirectional freeze-drying has been used to create uniquely structured porous materials by allowing ice crystals to form in both axial (bottom to top, similar to unidirectional freeze-drying) and radial (inwards toward the centre) directions.[89] The formation of radially aligned microchannels was achieved by using a metal container capable of conducting the temperature gradient from its walls into the sample (Fig. 5e). Cross-sectional side-views of the sponge reveal the different arrangements of GO nanosheets confirming the radially aligned aerogel that can be understood by the schematic provided (Fig. 5e). As seen in the SEM micrographs of Fig. 5f, different regions of the aerogel possess varied spacing between the GO nanosheets and thus, pore density differs locally within the sample. In addition to rate and direction of freezing, the properties of these sponges are also governed by GO nanosheets' size,[92] pH,[93] and humidity.[94] Ultralarge GO nanosheets are reported to yield a better alignment with ultralow percolation threshold, which when reduced, would make better electrical conductors.[92] At lower pH values (below 5.5, which is the pK_a of the majority of moieties on GO), most of GO's functional groups are protonated, interactions between nanosheets are stronger, and gelation can occur at a lower GO concentration. However, when mixed with other components, the scenario is not as simple. Pan *et al.* have reported that a mixture of equal mass ratios of 2,2,6,6-tetramethylpiperidin-1-oxyl, radical-mediated oxidized cellulose nanofibre (TOCN) and GO has a regular honeycomb structure at a pH of 5.2, where the overall repulsive electrostatic forces and attractive hydrogen-bonding interactions, along with GO/TOCN interactions with ice crystals are favourable for a hexagonal structure.[93] Mixtures with a lower pH (4.0) are described to have irregular structures due to attractive forces overcoming the repulsion, while those with higher pH (6.4 and 10.4) could have micro-lamella structure (greater repulsion causes larger distancing).

Nevertheless, sponges made using dispersions at low pH are known to possess higher storage modulus.[93] Relative humidity is found to affect the compression load afforded by freeze-dried sponges; the higher the relative humidity, the weaker the sponge would be, so it can withstand a smaller load and for a shorter period of time.[94]

Furthermore, it is reported that GO loses some of its oxygen-containing moieties during the freeze-drying process (increasing the C : O and $I_D : I_G$ ratios from ~1.6 to ~2.1 and 0.84 to 0.99, respectively).[95] While the loss of functional groups may not be sufficient to enhance the sponge's electrical conductivity without a pre- or follow up reduction procedure, the change is significant enough for the sponge to become hydrophobic and stable in water.[95] Freeze-drying is a well-studied methodology in forming porous graphene-based materials with a wide range of pore sizes. Therefore, the potential applications for graphene-based sponges obtained by this process can be very broad and include tissue engineering,[90] and environmental remediation[91] to name a few. Reduction of GO prior to or after freeze-drying results in a further increase of oxygen loss, decrease of interlayer spacing of GO nanosheets, and their conductive properties, making them suitable to be used in electronics and energy storage.[92] However, due to the high energy intake of the freeze-casting process, scalability of this method remains a challenge.[88,90,96]

3.2. 3D printing-freezing

With the limitations imposed by the freeze-drying methodology described above, the need to tailor macrostructures for specific applications at the scales desired has driven research developments on 3D printing (more specifically, "direct ink writing") of graphene-based sponges.[97] Compared to other techniques, additive layer-by-layer 3D printing could be used to better organize GO-based nanosheets into complex structures, such as filaments, thin films, (scrolled) fibers, membranes, porous collectors, *etc.* (Fig. 6).[98] There are, however, several key parameters to consider when fabricating a sponge using this methodology including the shear stresses in the nozzle intrinsically generated by shear-inducing flow, ink rheology, and the presence of a boundary-free controlled microstructure with a percolated 3D network within the sample. Moreover, the 3D printing process should not sacrifice the intrinsic properties of graphene-based nanosheets, such as their high specific surface area; therefore, careful deposition of the ink to achieve an ultralight density is desired.[99]

Three-dimensional printing has traditionally used a heating step to extrude the sample ink out at room temperature. While

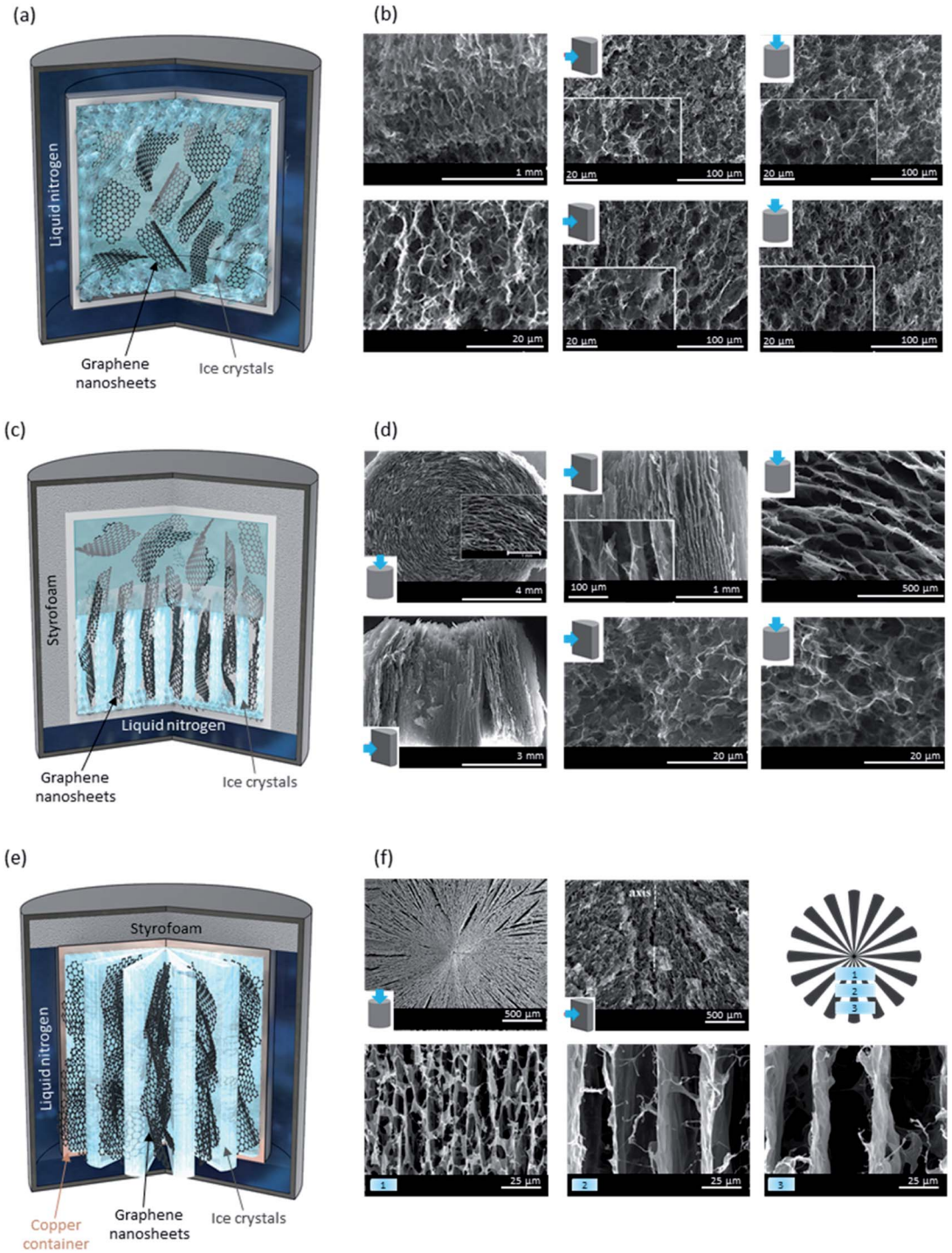

Fig. 5 (a) Schematic illustration of a bulk freeze-drying process. As shown here, ice crystals begin to form close to the container's walls and grow in random directions. (b) SEM micrographs of a bulk lyophilized GO-based aerogel, showing the randomness of pore architecture as a result of randomly formed ice crystals. Please note the insets in SEM images show the viewpoint of these porous materials (top *vs.* side view). (c) Schematic illustration of a unidirectional freeze-drying process. As shown, ice crystals begin to form from the liquid nitrogen side and grow upwards. (d) SEM micrographs of a unidirectionally lyophilized GO-based aerogel consisting of microchannels in the direction of ice crystal formation. (e) Schematic illustration of a bidirectional freeze-drying process. As shown, ice crystals form and grow in two directions: along the axis and radially, due to the usage of a temperature conductive container, such as copper. (f) SEM micrographs of a bidirectionally lyophilized GO-based aerogel display the formation of microchannels with different morphologies than those found in unidirectional freeze-drying. SEM images shown in the bottom row refer to different distances from the centre of the aerogel (regions numbered 1–3 and shown in the schematic). GO nanosheets are found to be more closely assembled near the centre of the aerogel. SEM images in 5b and 5d are adapted with permission from ref. 91 ©2019 American Chemical Society (2019). SEM images in (f) are adapted with permission from ref. 89 © 2018 American Chemical Society.

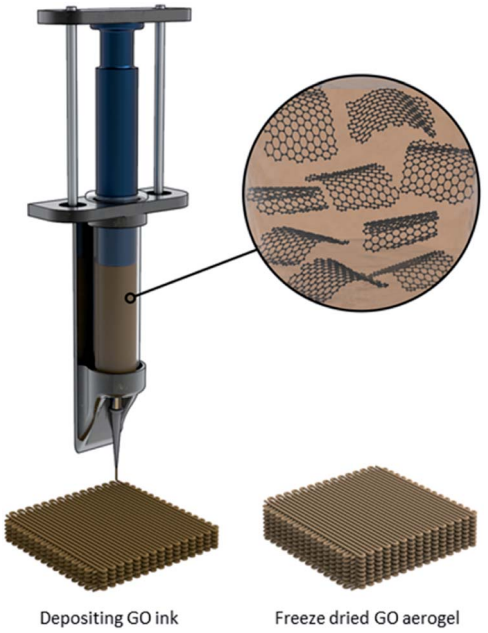

Fig. 6 Schematic illustration of a direct ink writing – a type of 3D printing process using GO ink (concentrated dispersion of GO in a solvent). Upon freeze-drying and removal of the solvent, a 3D porous GO aerogel is obtained, with porosity similar to that of freeze-dried aerogels.

the scalability of the extrusion is attractive, there are several challenges with controlling the architecture of the sponge using this method, such as changes in chemical properties of GO as high temperature is known to alter its chemical composition, as well as undesirable voids within the macrostructure. An approach reported by Lin *et al.*,[100] utilizes a freeze-gelation at room temperature. In this method, the nanosheets of interest are dispersed in an organic solvent with a melting point higher than room temperature and high vapour pressure. First, the nanosheets are dispersed in an appropriate solvent at a temperature higher than its melting point (*e.g.*, 60 °C for phenol) followed by cooling to room temperature, achieving a solid-state material. The high vapour pressure of this solvent enables for the rapid sublimation and thus, formation of a solid material with high porosity. While there is a need to heat up the suspension prior to deposition, one of the great advantages of this method is the variety of macrostructures one can obtain where there is no need of a container to freeze the solvent. In all the different 3D printing methodologies described here, removal of solvents is done by either freeze-drying, or critical point drying.[96,101,102]

Another strategy proposed by Zhang *et al.* combines the 3D printing of a GO suspension in water with simultaneous freeze-casting on a cold sink with temperature well below water's freezing point (−25 °C).[97] In this method, the printing is carried out by "drop-on-demand", meaning the GO suspension is ejected drop-by-drop. Since the suspension has a very low GO concentration, the final aerogel possesses a very low density and large surface area. The slow drop-on-demand technique preserves the intrinsic properties of the starting material by allowing the nanosheets to form a bond at the interface *via* intermolecular interactions, thus providing sufficient voids and pores between adjacent components. While the new GO suspension is deposited, since it is at room temperature, it melts the already frozen water level underneath, which not only facilitates the formation of hydrogen-bonding with the newly deposited GO nanosheets, but also fills the gap between the layers with the aid of surface tension and gravity. As shown in the SEM micrographs in Fig. 7, different regions of the macro-structure have distinctive pore morphologies. A comparison of this methodology with traditional 3D printing reveals that it enables higher precision and a more controlled porosity.[97] Moreover, the sponge has a 3D truss architecture with overhang structure, ultralight densities (0.5–10 mg mL^{-1}), significant electrical conductivity upon reduction (~15.4 S m^{-1}), high compressibility, and higher stiffness compared to other graphene-based aerogels with similar densities. The method is also found to be easier, more economically feasible, and less energy intensive, with a broad range of applications such as thermal insulators and strain sensors. In all the different 3D printing methodologies described here, removal of solvents is done by either freeze-drying, or critical point drying.[96,101,102]

Jiang *et al.* reported an ion-induced gelation method for direct ink writing of structures in air at room temperature. After

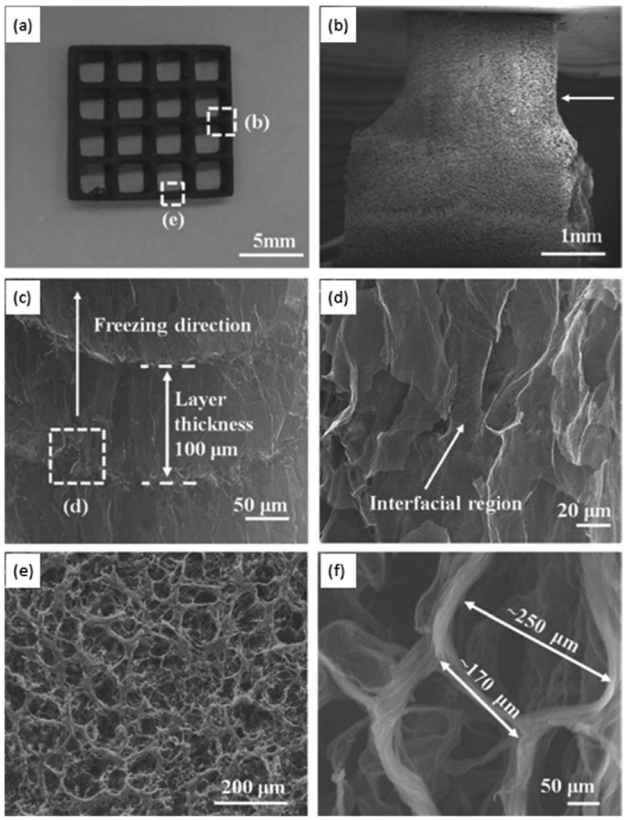

Fig. 7 (a) Photograph of a 3D printed sponge. SEM micrograph showing: (b) T-junction cut from (a), (c) morphology of the sponge along the deposition direction, (d) cross-sectional interfacial region in (c), (e) the top-view of the region in (a), and (f) morphology of the typical pores found in the aerogels. Figure reprinted with permission from ref. 97 © 2016 Wiley-VCH.

printing, GO microlattices were freeze-dried to obtain a solid GO aerogel with low density and high porosity.[101] The 2 wt% GO ink was prepared with micron-scale GO nanosheets (width of 5–20 μm) and 1.5×10^{-2} M $CaCl_2$ as crosslinker to yield favourable rheological properties (*i.e.*, viscosity, storage, loss and elastic moduli, and yield stress). Three-dimensional printing of GO nanowires at room temperature followed by reduction of GO by thermal or chemical treatment is also reported by Kim and co-authors.[102] The nanowire diameter was controlled (minimum value of 300 nm) by tuning the pulling rate of the nozzle (micropipette with 1.3 μm opening). Such precise nanoscale deposition technique is very promising for advanced electrical devices or for targeted adsorption in highly controlled/monitored reactors. Similarly, the inkjet method for GO-based composite could also be used to coat an existing skeleton with thin GO nanolayers to provide specific surface interactions for storage and/or removal of molecules, antibiotics, precious metals, contaminants, viruses, *etc.*[103]

3.3. Hard templating

This class of templates includes both colloidal particles and porous skeletons and can be safely assumed to be the most versatile type of templating as particles of different sizes and skeletons with various porosity can be selected.

3.3.1. Granule and bead-templating. In a bead-templated porous graphene-based material, pores and inter-layer spacings between the nanosheets are engineered based on the spaces occupied by the granules, as depicted in Fig. 8. Based on the sizes of colloidal particles used, nano-, micro-, milli- and hierarchically porous foams can be formed. Huang *et al.* reported mixing GO with 120 nm CH_3-silica spheres followed by calcination and HF etching as an effective method to yield such sponges with a total pore volume of ~4.3 $cm^3\ g^{-1}$ suitable to be used in bioanalysis and energy storage.[104] Deposition of iron nanoparticles onto these sponges is shown to have enhanced their magnetic properties that can be of interest in separation and delivery applications.[104]

Macroporous graphene-based 3D frameworks have been explored using different polymeric colloidal particles, such as polystyrene (PS) and poly(methyl methacrylate) (PMMA), as sacrificial templates. Choi *et al.* report the fabrication of such porous materials by first chemically modifying GO (CMG) by addition of ammonia and hydrazine solutions (partial reduction reaction); and then, mixing the CMG with 2 μm PS particles.[105] The mixture was then vacuum filtered and the free-standing films were peeled off from the filter paper. Finally, PS was removed from the films by immersing them in toluene. The embossed CMG (e-CMG) films were also coated with MnO_2. This final deposition step was carried out to enhance the electrical properties of the sponge and have it evaluated as a supercapacitor. The resulting sponge was shown to have potential as an energy storage device with high energy and power densities.

In another study, Chen *et al.* described the formation of a controllable regular graphene-based film by mixing GO suspension and PMMA latex spheres, followed by vacuum filtration.[106] The PMMA/GO film was then calcinated at 800 °C, to simultaneously decompose and remove the PMMA from the film and reduce GO. It was proposed that this 3D porous graphene-based film has the potential to be used in energy storage applications as a binder-free supercapacitor electrode with high-rate capability (10 V s^{-1}) and enhanced gravimetric capacitance.

In addition to the methodologies described thus far, there are other emerging approaches that can be further explored. Templating with water-soluble granules, such as vitamin C (VC), is one of these methods. In a study reported by Yousefi *et al.*, a dispersion of GO and CNC in water was mixed with different amounts of VC, which is also a reducing agent.[107] The mixture was then heated to 90 °C to reduce the GO and form the sponge. Depending on the amount of VC, the morphology of these sponges evolved from a uniformly porous sponge into a hierarchically porous structure with pores as large as millimeters in size. Since the large pores were only obtained when the amount of VC used was over its saturation point in water, they are believed to be the space that the VC granules had occupied prior to and during the reduction reaction. Follow-up studies further showed that the hierarchically porous VC-templated rGO sponge outperforms granular activated carbon in removing the model dye methylene blue in the presence and absence of natural organic matter.[108] Moreover, the antimicrobial performance of these VC-templated sponges were evaluated by functionalizing them with different antimicrobial agents.[109]

3.3.2. Coating porous substrates. Coating porous materials with graphene-based nanosheets followed by the removal of the skeleton, leaving a 3D porous graphene-based macrostructure is another approach taken by several researchers. Skeletons can be polymeric foams such as polyurethane,[110,111] or metallic frameworks, such as nickel-based[112,113] sponges. The advantage of this technique is that a material that can easily be made porous with

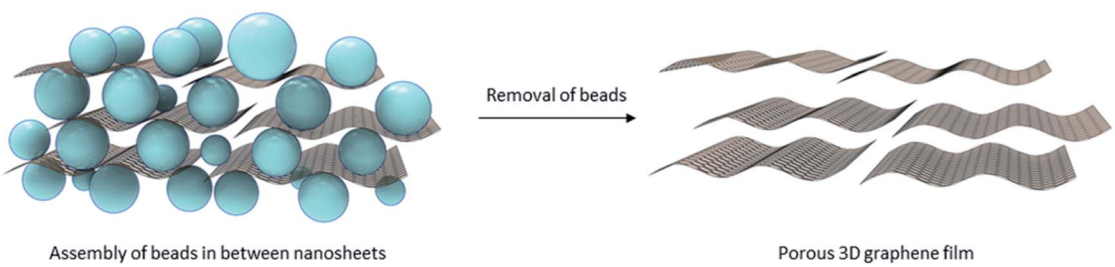

Fig. 8 Schematic illustration of beads' (nanoparticles or microspheres) localization in between nanosheets, creating ordered spacings. Removal of the beads results in formation of a 3D porous film with a porosity similar to the sizes of beads used.

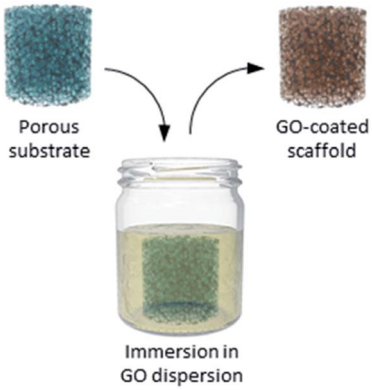

Fig. 9 Schematic illustration of coating a polymeric porous substrate with GO by simply immersing the substrate into the GO dispersion.

desired porosity and architecture is fabricated first, minimizing the limitations imposed when formulating a free-standing porous graphene-based material. Therefore, deserving attention can be given to the surface chemistry of the sponge, which originates from the graphene/GO coat, optimizing the adsorption capacity and other surface properties of such sponges. Needless to mention that selection of the porous skeleton is key in fabricating a porous GO-coated sponge, as efficiency of coating largely depends on the interactions between the skeleton and the GO nanosheets. This is especially important if physical coating is undertaken, whereby a polymeric porous substrate is immersed in a GO dispersion and electrostatic attractive forces become the sole governing interaction (Fig. 9). Alternatively, the coating step can be performed using chemical vapour deposition (CVD). CVD is a well-studied strategy to fabricate macroscopic 3D graphene foams using methane; however, since the focus of this review is on the development of such materials using GO as the base material, CVD is not further explained. While polymeric substrates can be utilized in several different applications, such as environmental remediation,[110,111,114–116] nickel-based skeletons coated with graphene are found to be promising nanomaterials used as electrodes and supercapacitors.[112,113]

3.4. Emulsion-templating

Emulsions are a group of soft materials where two immiscible liquids are mixed with the aid of a stabilizing agent, which can be a surfactant or nanoparticles.[117] In the case of nanoparticle-stabilized emulsions, if the nanoparticles are localized at the liquid–liquid interface (*e.g.* oil–water interface), the resultant emulsion is a Pickering emulsion.[118] However, nanoparticles may also just reside in one phase of the emulsion – the continuous phase – and still stabilize these systems.[118]

As GO is amphiphilic in nature, it has been used to stabilize several different immiscible mixtures such as oil/water emulsions and polymer blends.[119] The amphiphilicity of GO is a consequence of its carbon basal plane and the presence of many oxygen-containing functional groups on its surface. Therefore, the extent of amphiphilicity of GO depends on the nanosheets' sizes and pH. Large GO nanosheets have a low edge-to-area ratio and since the ionizable –COOH groups reside on the edges, their net charge is low. This idea was tested by He *et al.* as they observed a higher zeta potential value when sonicating GO dispersions and breaking large GO nanosheets.[120] Moreover, when used alone, GO nanosheets are more hydrophilic and better emulsifiers at low pH values as most functional groups are protonated. Overall, the following factors have been determined to influence GO emulsions' properties: size of GO sheets, oil/water ratios, oil phase composition, salinity, pH, and emulsification method as well as the presence of other emulsifying agents.[78]

With one phase dispersed in the other, one can imagine the formation of porous macrostructures by solidifying any of the internal or external phases. Traditionally, solidification of the material and removal of solvents can take place by polymerization of the phase of interest, forming different nanomaterials (Fig. 10). Polymerizing the dispersed phase can lead to the synthesis of beads and particles, as seen in the first reports of fabrication of PMMA-GO porous beads by Gudarzi *et al.* in 2011.[121] An ultimate porous material can be fabricated by fixing the nanoparticles in place – at the oil/water interface and/or in the continuous phase, solidifying the continuous phase, and removing the dispersed phase.[122] If both phases get polymerized (with different monomers), the final material is a composite. The latter is an area of particular interest when materials with specific properties are required but a single polymer cannot deliver the desired properties. In this case, a filler is used in the matrix of another polymer and forms a composite material.[37,123,124] Nonetheless, more recently, polymer-free emulsion-templated sponges have also been made.[125]

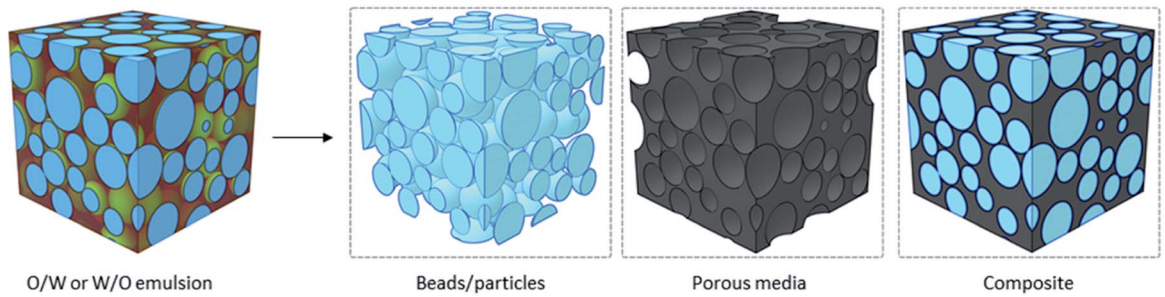

Fig. 10 Schematic illustration of three different nanomaterials that can be obtained by emulsion-templating: beads (*i.e.*, microspheres), porous media and composites.

3.4.1. Polymerized emulsion-templated: poly(HIPE). Emulsions whose dispersed phase makes up over 74% (v/v) of the mixture are considered as high internal phase emulsions (HIPE).[126–128] Synthesis of a porous structure can be achieved by gelling the continuous phase followed by removal of the internal liquid phase of HIPEs (Fig. 11a). The ultimate emulsion-templated porous material consists of pore sizes comparable to the droplet sizes of the dispersed phase and therefore, allows for tuning their microstructures. Polymerizing the external phase then results in the formation of a porous material with a porosity equal to the percentage of internal phase.[119] An advantage of this process is the preservation of the overall poly(HIPE) size. However, since a large portion of the starting material is polymerized and turned into a solid phase, there is a considerable surface area sacrifice which can be justified by the improvement in mechanical properties (*i.e.*, storage modulus and yield stress) of these 3D macrostructures. It has also been noted that the porosity of poly(HIPE)-based materials is interconnected.[119,129,130] This is especially attractive in applications where flow of another component is desired, such as ion flow in electrochemical applications,[129,131] or water flow in environmental remediation.[119,130]

3.4.2. Polymer-free emulsion-templating. Considering the limitations that the use of polymers imparts, researchers have also explored the possibility of not incorporating them. Jahandideh *et al.* recently reported the fabrication of polymer-free emulsion-templated sponges.[125] In this study, a cyclohexane-in-water emulsion was stabilized using GO and CNC in varying ratios. Emulsions were then mixed with vitamin C to reduce the GO and form the sponges (Fig. 11b). Favorable π–π interactions were enhanced by restoring sp^2 domains of graphene nanosheets.[125] Similar to the poly(HIPE) templated sponges, these macrostructures also possessed porosity similar to the droplet sizes. However, the absence of polymerization step resulted in an intensified stacking of the nanosheets and shrinkage in the final sponge's size. These polymer-free emulsion-templated sponges can be used in a range of applications including water treatment.[125]

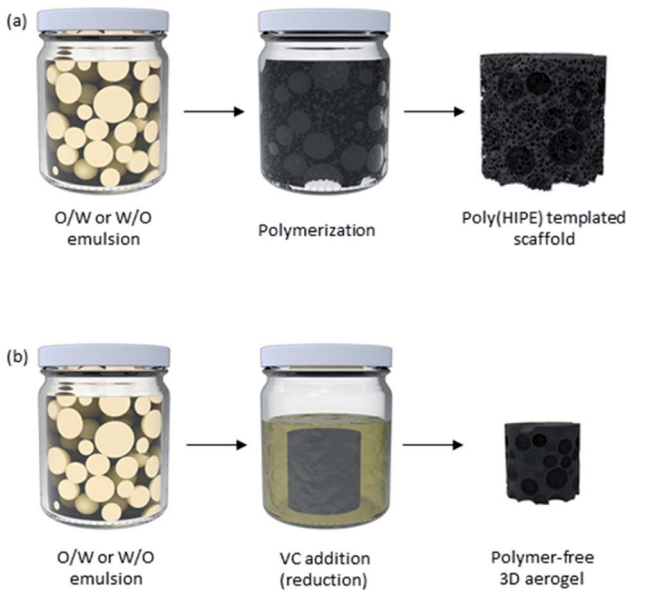

Fig. 11 (a) Schematic illustration of fabricating a 3D interconnected graphene-based porous material by templating a HIPE and polymerizing it into a poly(HIPE). (b) Schematic illustration of fabricating a 3D graphene-based porous material by templating an emulsion without the polymerization step and by reducing GO using vitamin C.

4. Technological, environmental, and economic feasibility considerations

Technological, environmental and economic feasibilities of a process play important roles in choosing the appropriate fabrication method, especially if scale-up is desired. On one hand, most template-free methodologies (*i.e.*, solvothermal and filtration) do not require state-of-the-art technologies and/or highly trained personnel to carry out the process. On the other hand, these processes either require significant energy inputs to achieve the necessary high temperature and pressures (in the case of solvothermal process) or large volumes of solvents (for filtration), making them both environmentally and economically unfavourable options. Though, recycling the solvent used in filtration may be a viable solution to improve this method's environmental impact. Cross-linking, as the remaining template-free option, requires advanced level of knowledge in surface chemistry and may need extreme experimental conditions in the case of chemical cross-linking (*e.g.*, high temperature, flammable solvents, *etc.*), making it an effective yet less desirable method, both economically and environmentally.

Ice-templating strategy is likely the only template-directed methodology that may not require a highly qualified personnel and/or an advanced technology other than a freeze-dryer. However, a cooling reagent, such as liquid nitrogen, is needed, and the energy intake of a freeze-dryer to effectively introduce vacuum and reduce temperature is significant. Therefore, this may not be a suitable method to form porous graphene-based macrostructures in large industrial scales. The remaining template-directed strategies of formation of graphene-based sponges (3D printing-freezing, hard-templating, and emulsion-templating) are technologically advanced and highly qualified personnel with specialized trainings are needed. In comparison with the other methods described in this review, the 3D printing-freezing technique requires a 3D printer, which is more technologically advanced. However, since this technique provides a highly adjustable deposition of the starting material and pore architecture of the final porous materials, the technology advancement may be justified for special applications (*e.g.*, bone tissue engineering). Hard-templating strategies (using both granules and porous substrates) are less technologically and economically demanding as they do not require advanced equipment, intensive energy inputs and/or challenging reaction conditions. However, etching out the particles and microspheres used in bead-templating may require hazardous organic solvents, making it a less environmentally friendly process. Choosing the

porous substrates wisely enables recyclability and economic benefits, making it a promising option for scale-up – especially for environmental remediation due to controllable pore sizes. Polymerization, in general, is a complex multi-step organic synthesis that may also need intensive reaction conditions, making the poly(HIPE)-templated scaffolds both technologically, and economically challenging. Depending on the solvents used, this method may also have a negative environmental impact. Replacing the polymerization step with addition of the green reducing agent vitamin C, is a promising yet underused modification to the strategy that improves the overall feasibility of this technique. However, this method requires a good temperature control during the reduction step and includes several washing steps to remove the unreacted VC and oil phase, that could potentially be better optimized.

As described thus far, balancing the three technological, environmental, and economic considerations is important and yet not practical. Therefore, a compromise on at least one of the factors is usually made in each process. Having environmental interests – which has societal impact – in mind, researchers are urged to explore the more advanced methodologies, such as 3D-printing-freezing and polymeric substrate coating of GO, where the structure of graphene-based macrostructure is optimized and tuned for the desired applications, while reducing the solvent waste and energy input of the processes. Optimization of these structures leads to expense reduction in the long-term and improves their economic feasibility as well.

5. General discussion and concluding remarks

Optimizing a graphene-based porous material suitable for a targeted application is a compromise between pore architecture, surface chemistry, mechanical properties, and scalability. Importantly, GO and its derivatives are being researched in materials design for their unique intrinsic properties including their exceptional specific surface area, as well as their mechanical, chemical, thermal, and electrical properties. Therefore, it is the ultimate goal in preparation of graphene-based sponges and hydrogels to achieve and maintain these characteristics as much as possible by using the minimum quantity of GO nanosheets. Fig. 12 shows the minimum GO content used in achieving different porosities using the different strategies described in this review. All methodologies except filtration, 3D-printing-freezing, and sponge coating can produce micro-sized (0.1–100 μm) pores using <10 mg mL^{-1} GO. Filtration, the process often used in making membranes and nano-sized (0.1–100 nm) films, is the only method that can form such small pores, nearly independent of the GO concentration. These small pore sizes were previously discussed to be the result of nanosheets' defects, and their wrinkles and interlayer spacings. This suggests that as long as the concentration of GO dispersion is within the explored dilute range, we can achieve the appropriate viscosity (<10 mPa s) to ensure that nanosheets are not overly stacked. Therefore, we can minimize the volume of required solvents and improve the

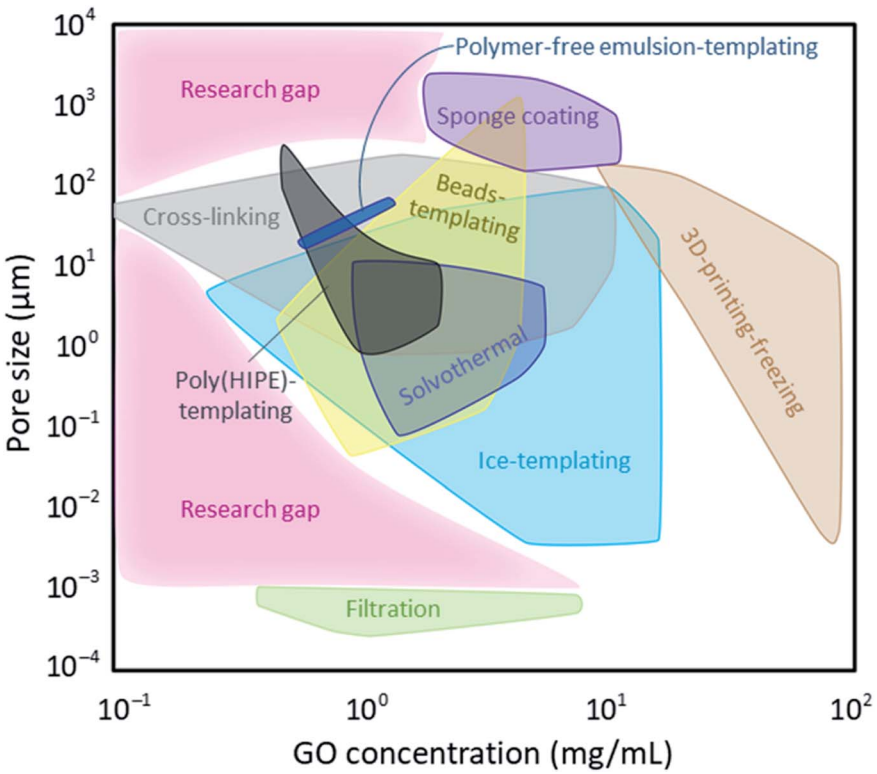

Fig. 12 Schematic representation of the relationship between the methodologies, GO concentration, and porous sizes of graphene-based porous materials using the available literature data. The pink areas outline the current research gaps.

environmental impact of this method. The pore sizes of porous substrates coated with graphene/GO are inherent to the pristine substrate prior to coating and independent of GO concentration. Nonetheless, the pore sizes of the commonly used skeletons fall on the larger end of the spectrum (0.1–5 mm). It is useful to highlight that the GO concentration reported for porous skeleton coating here refers to those used in the immersion approach and do not include CVD data as methane and carbon dioxide vapours are used in the latter as opposed to GO dispersions and could not be assessed in this analysis. Crosslinking GO nanosheets can form porous materials even at the low concentration of 0.1 mg mL^{-1}. This is mainly the case when different polymers are grafted onto GO nanosheets lowering the threshold of making their 3D network. Three-dimensional printing-freezing covers the higher end of GO concentration (10–100 mg mL^{-1}) since the viscosity of GO ink must be high enough to form a gel at room temperature. While this method allows for precise pore architecture, it sacrifices few of GO's intrinsic properties such as its outstanding specific surface area by promoting their stacking.

Fig. 12 can help us locate areas that are not explored yet (marked by pink and labeled as Research gap). These are the areas where lower GO concentrations could be used to achieve porous materials with different pore sizes suitable for various applications. We can name a few in environmental remediation as examples: small (nano) pores to be used in desalination and molecular sieves, large (micro and milli) pores to be implemented in oil spill cleanup and solvent absorption. Having the aforementioned information on properties and feasibility of these processes, we can identify areas requiring improvement. While most of these processes could be tuned and optimized to be more viable options for industrial scales, preservation of GO's intrinsic properties is also a must; therefore, processes capable of forming porous graphene-based materials using low GO concentrations (<1 mg mL^{-1}) are desired in most applications.

Author contributions

All authors contributed in reviewing literature, writing, and editing the article with H. J.'s leadership and N. T.'s supervision. H. J. and A. B. created the original figures of the article.

Conflicts of interest

N. T. holds a patent on the use of graphene sponges for water treatment. All other authors have no conflicts to declare.

Acknowledgements

The authors acknowledge the Canada Research Chairs program and the Natural Sciences and Engineering Research Council of Canada (NSERC). H. J. acknowledges the support of NSERC for a Canada Graduate Scholarship - Doctoral (CGS-D) and a CREATE award, as well as the McGill Engineering Doctoral Award (MEDA), Vadasz doctoral fellowship and Eugenie Ulmer-Lamothe (EUL) award. A. B. acknowledges the support from des Fonds Québécois de la Recherche sur la Nature et les Technologies (FRQNT) Doctoral Scholarship and a MEDA. M. L. acknowledges FRQNT and NSERC Postdoctoral Fellowships. J.-R. M acknowledges an NSERC Postdoctoral Fellowship.

References

1 K. Hu, X. Xie, M. Cerruti and T. Szkopek, Controlling the shell formation in hydrothermally reduced graphene hydrogel, *Langmuir*, 2015, **31**(20), 5545.
2 Y. Li, W. Cui, L. Liu, R. Zong, W. Yao, Y. Liang and Y. Zhu, Removal of Cr(VI) by 3D TiO 2 -graphene hydrogel *via* adsorption enriched with photocatalytic reduction, *Appl. Catal., B*, 2016, **199**, 412.
3 Y. Shen, Q. Fang and B. Chen, Environmental applications of three-dimensional graphene-based macrostructures: adsorption, transformation, and detection, *Environ. Sci. Technol.*, 2015, **49**(1), 67.
4 C. Zhu, P. Liu and A. P. Mathew, Self-Assembled TEMPO Cellulose Nanofibers: Graphene Oxide-Based Biohybrids for Water Purification, *ACS Appl. Mater. Interfaces*, 2017, **9**(24), 21048.
5 S. P. Surwade, S. N. Smirnov, I. V. Vlassiouk, R. R. Unocic, G. M. Veith, S. Dai and S. M. Mahurin, Water desalination using nanoporous single-layer graphene, *Nat. Nanotechnol.*, 2015, **10**(5), 459.
6 C. Yao, J. Yi, H. Lai, G. Shi, Y. Hu, Z. Chen, J. Zhai, X. Wang, L. Zhong and C. Liu, Enhancing the Mechanical Performance of Reduced Graphene Oxide Aerogel with Cellulose Nanofibers, *ChemNanoMat*, 2021, 7(8), 950.
7 X. Liu, K. Pang, H. Yang and X. Guo, Intrinsically microstructured graphene aerogel exhibiting excellent mechanical performance and super-high adsorption capacity, *Carbon*, 2020, **161**, 146.
8 C. Li, M. Ding, B. Zhang, X. Qiao and C.-Y. Liu, Graphene aerogels that withstand extreme compressive stress and strain, *Nanoscale*, 2018, **10**(38), 18291.
9 R. Singh, S. Ullah, N. Rao, M. Singh, I. Patra, D. A. Darko, C. P. J. Issac, K. Esmaeilzadeh-Salestani, R. Kanaoujiya and V. Vijayan, Synthesis of Three-Dimensional Reduced-Graphene Oxide from Graphene Oxide, *J. Nanomater.*, 2022, **2022**, 8731429.
10 N. Yousefi, X. Lu, M. Elimelech and N. Tufenkji, Environmental performance of graphene-based 3D macrostructures, *Nat. Nanotechnol.*, 2019, **14**(2), 107.
11 Y. Fadil, V. Agarwal, F. Jasinski, S. C. Thickett, H. Minami and P. B. Zetterlund, Electrically conductive polymer/rGO nanocomposite films at ambient temperature *via* miniemulsion polymerization using GO as surfactant, *Nanoscale*, 2019, **11**(14), 6566.
12 J. Jia, X. Sun, X. Lin, X. Shen, Y.-W. Mai and J.-K. Kim, Exceptional Electrical Conductivity and Fracture Resistance of 3D Interconnected Graphene Foam-Epoxy Composites, *ACS Nano*, 2014, **8**(6), 5774.
13 J. Kim, N. M. Han, J. Kim, J. Lee, J. K. Kim and S. Jeon, Highly Conductive and Fracture-Resistant Epoxy Composite Based on Non-oxidized Graphene Flake Aerogel, *ACS Appl. Mater. Interfaces*, 2018, **10**(43), 37507.

14 Y. Li, F. Xu, Z. Lin, X. Sun, Q. Peng, Y. Yuan, S. Wang, Z. Yang, X. He and Y. Li, Electrically and thermally conductive underwater acoustically absorptive graphene/rubber nanocomposites for multifunctional applications, *Nanoscale*, 2017, **9**(38), 14476.
15 Z. Yu, Z. Shi, H. Xu, X. Ma, M. Tian and J. Yin, Green chemistry: Co-assembly of tannin-assisted exfoliated low-defect graphene and epoxy natural rubber latex to form soft and elastic nacre-like film with good electrical conductivity, *Carbon*, 2017, **114**, 649.
16 F. Guo, M. Creighton, Y. Chen, R. Hurt and I. Kulaots, Porous Structures in Stacked, Crumpled and Pillared Graphene-Based 3D Materials, *Carbon N Y*, 2014, **66**, 476.
17 W. Lv, C. Zhang, Z. Li and Q.-H. Yang, Self-Assembled 3D Graphene Monolith from Solution, *J. Phys. Chem. Lett.*, 2015, **6**(4), 658.
18 Q. Zhang, X. Cheng, C. Wang, A. M. Rao and B. Lu, Sulfur-assisted large-scale synthesis of graphene microspheres for superior potassium-ion batteries, *Energy Environ. Sci.*, 2021, **14**(2), 965.
19 L. Fan, Y. Hu, A. M. Rao, J. Zhou, Z. Hou, C. Wang and B. Lu, Prospects of Electrode Materials and Electrolytes for Practical Potassium-Based Batteries, *Small Methods*, 2021, **5**(12), 2101131.
20 W. Hooch Antink, Y. Choi, K.-d. Seong, J. M. Kim and Y. Piao, Recent Progress in Porous Graphene and Reduced Graphene Oxide-Based Nanomaterials for Electrochemical Energy Storage Devices, *Adv. Mater. Interfaces*, 2018, **5**(5), 1701212.
21 Y. Xu, Z. Lin, X. Zhong, X. Huang, N. O. Weiss, Y. Huang and X. Duan, Holey graphene frameworks for highly efficient capacitive energy storage, *Nat. Commun.*, 2014, **5**(1), 4554.
22 M. G. Kochameshki, A. Marjani, M. Mahmoudian and K. Farhadi, Grafting of diallyldimethylammonium chloride on graphene oxide by RAFT polymerization for modification of nanocomposite polysulfone membranes using in water treatment, *Chem. Eng. J.*, 2017, **309**, 206.
23 R. Wu, B. Yu, X. Liu, H. Li, W. Wang, L. Chen, Y. Bai, Z. Ming and S.-T. Yang, One-pot hydrothermal preparation of graphene sponge for the removal of oils and organic solvents, *Appl. Surf. Sci.*, 2016, **362**, 56.
24 M. Tavafoghi, N. Brodusch, R. Gauvin and M. Cerruti, Hydroxyapatite formation on graphene oxide modified with amino acids: arginine *versus* glutamic acid, *J. R. Soc., Interface*, 2016, **13**(114), 20150986.
25 C. Sun, Y. Liu, J. Sheng, Q. Huang, W. Lv, G. Zhou and H.-M. Cheng, Status and prospects of porous graphene networks for lithium–sulfur batteries, *Mater. Horiz.*, 2020, **7**(10), 2487.
26 J. Han, W. Wei, C. Zhang, Y. Tao, W. Lv, G. Ling, F. Kang and Q.-H. Yang, Engineering Graphenes from the Nano- to the Macroscale for Electrochemical Energy Storage, *Electrochem. Energy Rev.*, 2018, **1**(2), 139.
27 A. Zaka, K. Hayat and V. Mittal, Recent Trends in the Use of Three-Dimensional Graphene Structures for Supercapacitors, *ACS Appl. Electron. Mater.*, 2021, **3**(2), 574.
28 C. Tang, H.-F. Wang, J.-Q. Huang, W. Qian, F. Wei, S.-Z. Qiao and Q. Zhang, 3D Hierarchical Porous Graphene-Based Energy Materials: Synthesis, Functionalization, and Application in Energy Storage and Conversion, *Electrochem. Energy Rev.*, 2019, **2**(2), 332.
29 Y. Wang, L. Guo, P. Qi, X. Liu and G. Wei, Synthesis of Three-Dimensional Graphene-Based Hybrid Materials for Water Purification: A Review, *Nanomaterials*, 2019, **9**(8), 1123.
30 C. Shao, Y. Zhao and L. Qu, Tunable Graphene Systems for Water Desalination, *ChemNanoMat*, 2020, **6**(7), 1028.
31 A. Hussain, M. Usman, R. Z. A. Manj, F. Liu, D. Li, and Y. Liu, Rational Design of Graphene-based Sorbents for Water Purification, *Nanostructured Catalysts for Environmental Applications*, 2021, 309.
32 M. Wu, L. Zou, L. Jiang, Z. Zhao and J. Liu, Osteoinductive and antimicrobial mechanisms of graphene-based materials for enhancing bone tissue engineering, *J. Tissue Eng. Regener. Med.*, 2021, **15**(11), 915.
33 X. Qi, F. Jiang, M. Zhou, W. Zhang and X. Jiang, Graphene oxide as a promising material in dentistry and tissue regeneration: A review, *Smart Mater. Med.*, 2021, **2**, 280.
34 C. Li, Z. Yang, Z. Tang, B. Guo, M. Tian and L. Zhang, A scalable strategy for constructing three-dimensional segregated graphene network in polymer *via* hydrothermal self-assembly, *Chem. Eng. J.*, 2019, **363**, 300.
35 E. Ou, X. Zhang, Z. Chen, Y. Zhan, Y. Du, G. Zhang, Y. Xiang, Y. Xiong and W. Xu, Macroscopic, free-standing Ag-reduced, graphene oxide Janus films prepared by evaporation-induced self-assembly, *Chemistry*, 2011, **17**(32), 8789.
36 Z. Tu, J. Wang, C. Yu, H. Xiao, T. Jiang, Y. Yang, D. Shi, Y.-W. Mai and R. K. Y. Li, A facile approach for preparation of polystyrene/graphene nanocomposites with ultra-low percolation threshold through an electrostatic assembly process, *Compos. Sci. Technol.*, 2016, **134**, 49.
37 Z. Wang, X. Shen, M. Akbari Garakani, X. Lin, Y. Wu, X. Liu, X. Sun and J. K. Kim, Graphene aerogel/epoxy composites with exceptional anisotropic structure and properties, *ACS Appl. Mater. Interfaces*, 2015, **7**(9), 5538.
38 Y. Xu, K. Sheng, C. Li and G. Shi, Self-Assembled Graphene Hydrogel *via* a One-Step Hydrothermal Process, *ACS Nano*, 2010, **4**(7), 4324.
39 S. X. Weng, N. Yousefi and N. Tufenkji, Self-Assembly of Ultralarge Graphene Oxide Nanosheets and Alginate into Layered Nanocomposites for Robust Packaging Materials, *ACS Appl. Nano Mater.*, 2019, **2**(3), 1431.
40 P. Zhang, J. Li, L. Lv, Y. Zhao and L. Qu, Vertically Aligned Graphene Sheets Membrane for Highly Efficient Solar Thermal Generation of Clean Water, *ACS Nano*, 2017, **11**(5), 5087.
41 W. Deng, Q. Fang, X. Zhou, H. Cao and Z. Liu, Hydrothermal self-assembly of graphene foams with controllable pore size, *RSC Adv.*, 2016, **6**(25), 20843.
42 G. Demazeau, Solvothermal reactions: an original route for the synthesis of novel materials, *J. Mater. Sci.*, 2008, **43**(7), 2104.

43 S. G. Sergey Dubin, K. Wang, V. C. Tung, K. Cha, A. S. Hall, J. Farrar, R. Varshneya, Y. Yang and R. B. Kaner, A one-step, solvothermal reduction method for producing reduced graphene oxide dispersions in organic solvents, *ACS Nano*, 2010, **4**(7), 3845.

44 H. P. Mungse, O. P. Sharma, H. Sugimura and O. P. Khatri, Hydrothermal deoxygenation of graphene oxide in sub- and supercritical water, *RSC Adv.*, 2014, **4**(43), 22589.

45 B. Xu, S. Yue, Z. Sui, X. Zhang, S. Hou, G. Cao and Y. Yang, What is the choice for supercapacitors: graphene or graphene oxide?, *Energy Environ. Sci.*, 2011, **4**(8), 2826.

46 K. Hu, X. Xie, T. Szkopek and M. Cerruti, Understanding Hydrothermally Reduced Graphene Oxide Hydrogels: From Reaction Products to Hydrogel Properties, *Chem. Mater.*, 2016, **28**(6), 1756.

47 J. Zhao, W. Ren and H.-M. Cheng, Graphene sponge for efficient and repeatable adsorption and desorption of water contaminations, *J. Mater. Chem.*, 2012, **22**(38), 20197.

48 Y. Xu, Z. Lin, X. Huang, Y. Liu, Y. Huang and X. Duan, Flexible Solid-State Supercapacitors Based on Three-Dimensional Graphene Hydrogel Films, *ACS Nano*, 2013, **7**(5), 4042.

49 J. Shen, M. Zhang, G. Liu, K. Guan and W. Jin, Size effects of graphene oxide on mixed matrix membranes for CO2 separation, *AIChE J.*, 2016, **62**(8), 2843.

50 D. A. Dikin, S. Stankovich, E. J. Zimney, R. D. Piner, G. H. B. Dommett, G. Evmenenko, S. T. Nguyen and R. S. Ruoff, Preparation and characterization of graphene oxide paper, *Nature*, 2007, **448**(7152), 457.

51 C.-H. Tsou, Q.-F. An, S.-C. Lo, M. De Guzman, W.-S. Hung, C.-C. Hu, K.-R. Lee and J.-Y. Lai, Effect of microstructure of graphene oxide fabricated through different self-assembly techniques on 1-butanol dehydration, *J. Membr. Sci.*, 2015, **477**, 93.

52 S. Wang, Y. Wu, N. Zhang, G. He, Q. Xin, X. Wu, H. Wu, X. Cao, M. D. Guiver and Z. Jiang, A highly permeable graphene oxide membrane with fast and selective transport nanochannels for efficient carbon capture, *Energy Environ. Sci.*, 2016, **9**(10), 3107.

53 J. Shen, G. Liu, K. Huang, Z. Chu, W. Jin and N. Xu, Subnanometer Two-Dimensional Graphene Oxide Channels for Ultrafast Gas Sieving, *ACS Nano*, 2016, **10**(3), 3398.

54 F. Wang and J. Liu, Evaporation induced wrinkling of graphene oxide at the nanoparticle interface, *Nanoscale*, 2015, **7**(3), 919.

55 M. Coleman and X. Tang, Diffusive transport of two charge equivalent and structurally similar ruthenium complex ions through graphene oxide membranes, *Nano Res.*, 2015, **8**(4), 1128.

56 S. Huang, M. Dakhchoune, W. Luo, E. Oveisi, G. He, M. Rezaei, J. Zhao, D. T. L. Alexander, A. Züttel, M. S. Strano, *et al.*, Single-layer graphene membranes by crack-free transfer for gas mixture separation, *Nat. Commun.*, 2018, **9**(1), 2632.

57 J. Lyu, X. Wen, U. Kumar, Y. You, V. Chen and R. K. Joshi, Separation and purification using GO and r-GO membranes, *RSC Adv.*, 2018, **8**(41), 23130.

58 B. Motevalli, B. Sun and A. S. Barnard, Understanding and Predicting the Cause of Defects in Graphene Oxide Nanostructures Using Machine Learning, *J. Phys. Chem. C*, 2020, **124**(13), 7404.

59 O. Kwon, Y. Choi, E. Choi, M. Kim, Y. C. Woo and D. W. Kim, Fabrication Techniques for Graphene Oxide-Based Molecular Separation Membranes: Towards Industrial Application, *Nanomaterials*, 2021, **11**(3), 757.

60 J. Ma, D. Ping and X. Dong, Recent Developments of Graphene Oxide-Based Membranes: A Review, *Membranes*, 2017, **7**(3), 52.

61 R. K. Joshi, P. Carbone, F. C. Wang, V. G. Kravets, Y. Su, I. V. Grigorieva, H. A. Wu, A. K. Geim and R. R. Nair, Precise and Ultrafast Molecular Sieving Through Graphene Oxide Membranes, *Science*, 2014, **343**(6172), 752.

62 J. Heo, M. Choi, J. Chang, D. Ji, S. W. Kang and J. Hong, Highly Permeable Graphene Oxide/Polyelectrolytes Hybrid Thin Films for Enhanced CO2/N2 Separation Performance, *Sci. Rep.*, 2017, **7**(1), 456.

63 B. D. Freeman, Basis of Permeability/Selectivity Tradeoff Relations in Polymeric Gas Separation Membranes, *Macromolecules*, 1999, **32**(2), 375.

64 M. Liu, P. J. Weston and R. H. Hurt, Controlling nanochannel orientation and dimensions in graphene-based nanofluidic membranes, *Nat. Commun.*, 2021, **12**(1), 507.

65 S. J. Gao, H. Qin, P. Liu and J. Jin, SWCNT-intercalated GO ultrathin films for ultrafast separation of molecules, *J. Mater. Chem. A*, 2015, **3**(12), 6649.

66 W. Wang, E. Eftekhari, G. Zhu, X. Zhang, Z. Yan and Q. Li, Graphene oxide membranes with tunable permeability due to embedded carbon dots, *Chem. Commun.*, 2014, **50**(86), 13089.

67 S. Liu, M. Cerruti and F. Barthelat, Plastic Forming of Graphene Oxide Membranes into 3D Structures, *ACS Nano*, 2020, **14**(11), 15936.

68 H.-P. Cong, X.-C. Ren, P. Wang and S.-H. Yu, Macroscopic Multifunctional Graphene-Based Hydrogels and Aerogels by a Metal Ion Induced Self-Assembly Process, *ACS Nano*, 2012, **6**(3), 2693.

69 H. Bai, K. Sheng, P. Zhang, C. Li and G. Shi, Graphene oxide/conducting polymer composite hydrogels, *J. Mater. Chem.*, 2011, **21**(46), 18653–18658.

70 S. H. Lee, H. W. Kim, J. O. Hwang, W. J. Lee, J. Kwon, C. W. Bielawski, R. S. Ruoff and S. O. Kim, Three-dimensional self-assembly of graphene oxide platelets into mechanically flexible macroporous carbon films, *Angew. Chem., Int. Ed. Engl.*, 2010, **49**(52), 10084.

71 Y. Jeong, H. Ryu, C. Choi, S. An, W. Kim, D. Kim, B. Choi, B. K. Salunke and B. S. Kim, Characteristics of Graphene Production from Graphite using Plant Extracts, *KSBB Journal*, 2016, **31**(4), 208.

72 H. Gholipour-Ranjbar, M. R. Ganjali, P. Norouzi and H. R. Naderi, Synthesis of cross-linked graphene aerogel/

Fe2O3 nanocomposite with enhanced supercapacitive performance, *Ceram. Int.*, 2016, **42**(10), 12097.

73 Q. Zheng, Z. Cai, Z. Ma and S. Gong, Cellulose nanofibril/reduced graphene oxide/carbon nanotube hybrid aerogels for highly flexible and all-solid-state supercapacitors, *ACS Appl. Mater. Interfaces*, 2015, **7**(5), 3263.

74 X. Jiang, Y. Ma, J. Li, Q. Fan and W. Huang, Self-assembly of reduced graphene oxide into three-dimensional architecture by divalent ion linkage, *J. Phys. Chem. C*, 2010, **114**, 22462.

75 Y. Chen, L. Chen, H. Bai and L. Li, Graphene oxide–chitosan composite hydrogels as broad-spectrum adsorbents for water purification, *J. Mater. Chem. A*, 2013, **1**(6), 1992.

76 D. Han, P. Xiao, J. Gu, J. Chen, Z. Cai, J. Zhang, W. Wang and T. Chen, Polymer brush functionalized Janus graphene oxide/chitosan hybrid membranes, *RSC Adv.*, 2014, **4**(43), 22759.

77 R. Yu, Y. Shi, D. Yang, Y. Liu, J. Qu and Z. Z. Yu, Graphene Oxide/Chitosan Aerogel Microspheres with Honeycomb-Cobweb and Radially Oriented Microchannel Structures for Broad-Spectrum and Rapid Adsorption of Water Contaminants, *ACS Appl. Mater. Interfaces*, 2017, **9**(26), 21809.

78 H. Jahandideh, P. Ganjeh-Anzabi, S. L. Bryant and M. Trifkovic, The Significance of Graphene Oxide-Polyacrylamide Interactions on the Stability and Microstructure of Oil-in-Water Emulsions, *Langmuir*, 2018, **34**(43), 12870.

79 M.-m. Cheng, L.-j. Huang, Y.-x. Wang, Y.-c. Zhao, J.-g. Tang, Y. Wang, Y. Zhang, M. Hedayati, M. J. Kipper and S. R. Wickramasinghe, Synthesis of graphene oxide/polyacrylamide composite membranes for organic dyes/water separation in water purification, *J. Mater. Sci.*, 2018, **54**(1), 252.

80 H. P. Cong, P. Wang and S. H. Yu, Highly elastic and superstretchable graphene oxide/polyacrylamide hydrogels, *Small*, 2014, **10**(3), 448.

81 J. Fan, Z. Shi, M. Lian, H. Li and J. Yin, Mechanically strong graphene oxide/sodium alginate/polyacrylamide nanocomposite hydrogel with improved dye adsorption capacity, *J. Mater. Chem. A*, 2013, **1**(25), 7433.

82 R. Liu, S. Liang, X.-Z. Tang, D. Yan, X. Li and Z.-Z. Yu, Tough and highly stretchable graphene oxide/polyacrylamide nanocomposite hydrogels, *J. Mater. Chem.*, 2012, **22**(28), 14160–14167.

83 J. Shen, B. Yan, T. Li, Y. Long, N. Li and M. Ye, Study on graphene-oxide-based polyacrylamide composite hydrogels, *Composites, Part A*, 2012, **43**(9), 1476.

84 Y. Yang, S. Song and Z. Zhao, Graphene oxide (GO)/polyacrylamide (PAM) composite hydrogels as efficient cationic dye adsorbents, *Colloids Surf., A*, 2017, **513**, 315.

85 N. Zhang, R. Li, L. Zhang, H. Chen, W. Wang, Y. Liu, T. Wu, X. Wang, W. Wang, Y. Li, *et al.*, Actuator materials based on graphene oxide/polyacrylamide composite hydrogels prepared by *in situ* polymerization, *Soft Matter*, 2011, **7**(16), 7231–7239.

86 Q. Fang and B. Chen, Self-assembly of graphene oxide aerogels by layered double hydroxides cross-linking and their application in water purification, *J. Mater. Chem. A*, 2014, **2**(23), 8941.

87 K. Zhao, T. Zhang, H. Chang, Y. Yang, P. Xiao, H. Zhang, C. Li, C. S. Tiwary, P. M. Ajayan and Y. Chen, Super-elasticity of three-dimensionally cross-linked graphene materials all the way to deep cryogenic temperatures, *Sci. Adv.*, 2019, **5**(4), eaav2589.

88 Y. Li, H. Zhang, M. Fan, J. Zhuang and L. Chen, A robust salt-tolerant superoleophobic aerogel inspired by seaweed for efficient oil-water separation in marine environments, *Phys. Chem. Chem. Phys.*, 2016, **18**(36), 25394.

89 C. Wang, X. Chen, B. Wang, M. Huang, B. Wang, Y. Jiang and R. S. Ruoff, Freeze-Casting Produces a Graphene Oxide Aerogel with a Radial and Centrosymmetric Structure, *ACS Nano*, 2018, **12**(6), 5816.

90 C. Valencia, C. H. Valencia, F. Zuluaga, M. E. Valencia, J. H. Mina and C. D. Grande-Tovar, Synthesis and Application of Scaffolds of Chitosan-Graphene Oxide by the Freeze-Drying Method for Tissue Regeneration, *Molecules*, 2018, **23**(10), 2651.

91 V. Rodríguez-Mata, J. M. González-Domínguez, A. M. Benito, W. K. Maser and E. García-Bordejé, Reduced Graphene Oxide Aerogels with Controlled Continuous Microchannels for Environmental Remediation, *ACS Appl. Nano Mater.*, 2019, **2**(3), 1210.

92 N. M. Han, Z. Wang, X. Shen, Y. Wu, X. Liu, Q. Zheng, T. H. Kim, J. Yang and J. K. Kim, Graphene Size-Dependent Multifunctional Properties of Unidirectional Graphene Aerogel/Epoxy Nanocomposites, *ACS Appl. Mater. Interfaces*, 2018, **10**(7), 6580.

93 Z. Z. Pan, A. Govedarica, H. Nishihara, R. Tang, C. Wang, Y. Luo, W. Lv, F. Y. Kang, M. Trifkovic and Q. H. Yang, pH-Dependent Morphology Control of Cellulose Nanofiber/Graphene Oxide Cryogels, *Small*, 2021, **17**(3), e2005564.

94 R. Ming, Y. Ding, F. Chang, X. He, J. Feng, C. Wang and P. Zhang, Humidity-dependant compression properties of graphene oxide foams prepared by freeze-drying technique, *Micro Nano Lett.*, 2013, **8**(2), 66.

95 H. Ham, T. V. Khai, N. H. Park, D. S. So, J. W. Lee, H. G. Na, Y. J. Kwon, H. Y. Cho and H. W. Kim, Freeze-drying-induced changes in the properties of graphene oxides, *Nanotechnology*, 2014, **25**(23), 235601.

96 C. Ding, Y. Zhao, D. Yan, Y. Zhao, H. Zhou, J. Li and H. Jin, An Insight into the Convenience and Efficiency of the Freeze-Drying Route to Construct 3D Graphene-Based Hybrids for Lithium-Ion Batteries, *Electrochim. Acta*, 2016, **221**, 124.

97 Q. Zhang, F. Zhang, S. P. Medarametla, H. Li, C. Zhou and D. Lin, 3D Printing of Graphene Aerogels, *Small*, 2016, **12**(13), 1702.

98 P. Liu, Z. Jin, G. Katsukis, L. W. Drahushuk, S. Shimizu, C.-J. Shih, E. D. Wetzel, J. K. Taggart-Scarff, B. Qing, K. J. V. Vliet, *et al.*, Layered and scrolled nanocomposites

with aligned semi-infinite graphene inclusions at the platelet limit, *Science*, 2016, **353**(6297), 364.

99 B. Yao, S. Chandrasekaran, H. Zhang, A. Ma, J. Kang, L. Zhang, X. Lu, F. Qian, C. Zhu, E. B. Duoss, *et al.*, 3D-Printed Structure Boosts the Kinetics and Intrinsic Capacitance of Pseudocapacitive Graphene Aerogels, *Adv. Mater.*, 2020, **32**(8), e1906652.

100 Y. Lin, F. Liu, G. Casano, R. Bhavsar, I. A. Kinloch and B. Derby, Pristine Graphene Aerogels by Room-Temperature Freeze Gelation, *Adv. Mater.*, 2016, **28**(36), 7993.

101 Y. Jiang, Z. Xu, T. Huang, Y. Liu, F. Guo, J. Xi, W. Gao and C. Gao, Direct 3D Printing of Ultralight Graphene Oxide Aerogel Microlattices, *Adv. Funct. Mater.*, 2018, **28**(16), 1707024.

102 J. H. Kim, W. S. Chang, D. Kim, J. R. Yang, J. T. Han, G. W. Lee, J. T. Kim and S. K. Seol, 3D printing of reduced graphene oxide nanowires, *Adv. Mater.*, 2015, **27**(1), 157.

103 N. Karim, S. Afroj, S. Tan, K. S. Novoselov and S. G. Yeates, All Inkjet-Printed Graphene-Silver Composite Ink on Textiles for Highly Conductive Wearable Electronics Applications, *Sci. Rep.*, 2019, **9**(1), 8035.

104 X. Huang, K. Qian, J. Yang, J. Zhang, L. Li, C. Yu and D. Zhao, Functional nanoporous graphene foams with controlled pore sizes, *Adv. Mater.*, 2012, **24**(32), 4419.

105 B. G. Choi, M. Yang, W. H. Hong, J. W. Choi and Y. S. Huh, 3D macroporous graphene frameworks for supercapacitors with high energy and power densities, *ACS Nano*, 2012, **6**(5), 4020.

106 C. M. Chen, Q. Zhang, C. H. Huang, X. C. Zhao, B. S. Zhang, Q. Q. Kong, M. Z. Wang, Y. G. Yang, R. Cai and D. Sheng Su, Macroporous 'bubble' graphene film *via* template-directed ordered-assembly for high rate supercapacitors, *Chem. Commun.*, 2012, **48**(57), 7149.

107 N. Yousefi, K. K. W. Wong, Z. Hosseinidoust, H. O. Sørensen, S. Bruns, Y. Zheng and N. Tufenkji, Hierarchically porous, ultra-strong reduced graphene oxide-cellulose nanocrystal sponges for exceptional adsorption of water contaminants, *Nanoscale*, 2018, **10**, 7171.

108 R. Allgayer, N. Yousefi and N. Tufenkji, Graphene oxide sponge as adsorbent for organic contaminants: comparison with granular activated carbon and influence of water chemistry, *Environ. Sci.: Nano*, 2020, **7**(9), 2669.

109 A. Filina, N. Yousefi, M. Okshevsky and N. Tufenkji, Antimicrobial Hierarchically Porous Graphene Oxide Sponges for Water Treatment, *ACS Appl. Bio Mater.*, 2019, **2**(4), 1578.

110 Y. J. Kim, H. J. Kang, C. T. Moerk, B.-T. Lee, J. S. Choi and J.-H. Yim, Flexible, biocompatible, and electroconductive Polyurethane foam composites coated with graphene oxide for ammonia detection, *Sens. Actuators, B*, 2021, **344**, 130269.

111 Y. Liu, J. Ma, T. Wu, X. Wang, G. Huang, Y. Liu, H. Qiu, Y. Li, W. Wang and J. Gao, Cost-effective reduced graphene oxide-coated polyurethane sponge as a highly efficient and reusable oil-absorbent, *ACS Appl. Mater. Interfaces*, 2013, **5**(20), 10018.

112 F. Zhang, D. Zhu, X. Chen, X. Xu, Z. Yang, C. Zou, K. Yang and S. Huang, A nickel hydroxide-coated 3D porous graphene hollow sphere framework as a high performance electrode material for supercapacitors, *Phys. Chem. Chem. Phys.*, 2014, **16**(9), 4186.

113 X. Xiao, J. R. Michael, T. Beechem, A. McDonald, M. Rodriguez, M. T. Brumbach, T. N. Lambert, C. M. Washburn, J. Wang, S. M. Brozik, *et al.*, Three dimensional nickel–graphene core–shell electrodes, *J. Mater. Chem.*, 2012, **22**(45), 23749.

114 H. Kim, Y. Miura and C. W. Macosko, Graphene/Polyurethane Nanocomposites for Improved Gas Barrier and Electrical Conductivity, *Chem. Mater.*, 2010, **22**(11), 3441.

115 K.-H. Liao, Y. Qian and C. W. Macosko, Ultralow percolation graphene/polyurethane acrylate nanocomposites, *Polymer*, 2012, **53**(17), 3756.

116 J. H. Oh, J. Kim, H. Lee, Y. Kang and I. K. Oh, Directionally Antagonistic Graphene Oxide-Polyurethane Hybrid Aerogel as a Sound Absorber, *ACS Appl. Mater. Interfaces*, 2018, **10**(26), 22650.

117 Y. T. Hu, Y. Ting, J. Y. Hu and S. C. Hsieh, Techniques and methods to study functional characteristics of emulsion systems, *J. Food Drug Anal.*, 2017, **25**(1), 16.

118 B. K. Pilapil, H. Jahandideh, S. L. Bryant and M. Trifkovic, Stabilization of Oil-in-Water Emulsions with Noninterfacially Adsorbed Particles, *Langmuir*, 2016, **32**(28), 7109.

119 Z. Zheng, X. Zheng, H. Wang and Q. Du, Macroporous graphene oxide-polymer composite prepared through pickering high internal phase emulsions, *ACS Appl. Mater. Interfaces*, 2013, **5**(16), 7974.

120 Y. He, F. Wu, X. Sun, R. Li, Y. Guo, C. Li, L. Zhang, F. Xing, W. Wang and J. Gao, Factors that affect Pickering emulsions stabilized by graphene oxide, *ACS Appl. Mater. Interfaces*, 2013, **5**(11), 4843.

121 M. M. Gudarzi and F. Sharif, Self assembly of graphene oxide at the liquid–liquid interface: A new route to the fabrication of graphene based composites, *Soft Matter*, 2011, **7**(7), 3432.

122 H. Zhang and A. I. Cooper, Synthesis and applications of emulsion-templated porous materials, *Soft Matter*, 2005, **1**(2), 107.

123 H. Kim, S. Kobayashi, M. A. AbdurRahim, M. J. Zhang, A. Khusainova, M. A. Hillmyer, A. A. Abdala and C. W. Macosko, Graphene/polyethylene nanocomposites: Effect of polyethylene functionalization and blending methods, *Polymer*, 2011, **52**(8), 1837.

124 L. Embrey, P. Nautiyal, A. Loganathan, A. Idowu, B. Boesl and A. Agarwal, Three-Dimensional Graphene Foam Induces Multifunctionality in Epoxy Nanocomposites by Simultaneous Improvement in Mechanical, Thermal, and Electrical Properties, *ACS Appl. Mater. Interfaces*, 2017, **9**(45), 39717.

125 H. Jahandideh, Q. A. Nguyen and N. Tufenkji, Polymer-Free Emulsion-Templated Graphene-Based Sponges for Contaminant Removal, *ACS Appl. Mater. Interfaces*, 2020, **12**(46), 52095.

126 S. Ansari and E. P. Giannelis, Functionalized graphene sheet-poly(vinylidene fluoride) conductive nanocomposites, *J. Polym. Sci., Part B: Polym. Phys.*, 2009, **47**(9), 888.

127 T. D. Dao, G. Erdenedelger and H. M. Jeong, Water-dispersible graphene designed as a Pickering stabilizer for the suspension polymerization of poly(methyl methacrylate)/graphene core–shell microsphere exhibiting ultra-low percolation threshold of electrical conductivity, *Polymer*, 2014, **55**(18), 4709.

128 C. Gao, P. Liu, Y. Ding, T. Li, F. Wang, J. Chen, S. Zhang, Z. Li and M. Yang, Non-contact percolation of unstable graphene networks in poly(styrene-co-acrylonitrile) nanocomposites: electrical and rheological properties, *Compos. Sci. Technol.*, 2018, **155**, 41.

129 J. Wang, H. Hu, X. Wang, C. Xu, M. Zhang and X. Shang, Preparation and mechanical and electrical properties of graphene nanosheets-poly(methyl methacrylate) nanocomposites *via in situ* suspension polymerization, *J. Appl. Polym. Sci.*, 2011, **122**(3), 1866.

130 W. Yi, H. Wu, H. Wang and Q. Du, Interconnectivity of Macroporous Hydrogels Prepared *via* Graphene Oxide-Stabilized Pickering High Internal Phase Emulsions, *Langmuir*, 2016, **32**(4), 982.

131 V. H. Pham, T. T. Dang, S. H. Hur, E. J. Kim and J. S. Chung, Highly conductive poly(methyl methacrylate) (PMMA)-reduced graphene oxide composite prepared by self-assembly of PMMA latex and graphene oxide through electrostatic interaction, *ACS Appl. Mater. Interfaces*, 2012, **4**(5), 2630.